Publishing Excellence
Inspiring Progress
ARISTON PUBLICATIONS
ChemSci Advances
ISSN: 2997-9587 www.aristonpubs.com/chemsci-advances https://doi.org/10.69626/csa.2024.0111

RESEARCH ARTICLE

Structural and Anticoagulant studies of $Mg_{1-x}Zn_xFe_2O_4$, $Mg_{1-x}Co_xFe_2O_4$ and $Mg_{1-x}Ni_xFe_2O_4$ (x=0.15, 0.25 and 0.35) ferrites synthesized by Co-precipitation

Rakesh Vishwarup[1], Shridhar N. Mathad[2*], S. Nagaraju[3], Sandip V. Kamat[4], Deepak B. Shirgaonkar[5*]

ABSTRACT: $Mg_{1-x}Zn_xFe_2O_4$, $Mg_{1-x}Co_xFe_2O_4$, and $Mg_{1-x}Ni_xFe_2O_4$ ferrites synthesized by using Co-precipitation method. The structural characterizations of these samples were carried out and the formation of single phase ferrite was substantiated through powder X-ray diffraction (XRD), which revealed single phase cubic spinel structure, with lattice constants ranging from 8.323 to 8.353 Å, 8.328 to 8.351 Å, and 8.315 to 8.366 Å for the $Mg_{1-x}Zn_xFe_2O_4$, $Mg_{1-x}Co_xFe_2O_4$, and $Mg_{1-x}Ni_xFe_2O_4$ ferrites, respectively. Surface morphology was investigated through scanning electron microscopic (SEM) analysis. The grain sizes for the $Mg_{1-x}Zn_xFe_2O_4$, $Mg_{1-x}Co_xFe_2O_4$, and $Mg_{1-x}Ni_xFe_2O_4$ ferrites were found to vary from 3.745 to 4.227 µm, 4.034 to 5.08 µm, and 3.946 to 4.887 µm, respectively. The prepared samples showed high anticoagulant properties for the highest concentration of dopant proved by re-calcification time (RT), prothrombin time (PT) and platelet aggregation measurements. The higher RT, PT and Activated partial thromboplastin time (aPPT) values for the x=0.35 ferrites and lower platelet aggregation of the x=0.35 ferrites reveal that the anticoagulant properties of the x=0.35 ferrites are superior to those of the x=0.15 and x=0.25 ferrites for all samples.

Keywords: Magnesium Ferrite, anticoagulant, Co-precipitation method, prothrombin time.

Received: 13 March 2024; Revised: 21 April 2024; Accepted: 15 May 2024; Published Online: 15 June 2024

1. INTRODUCTION

Synthesis of the nanomaterials has attracted wide attention due to their surface effect and quantum confinement effect. These factors are modifying the physical and chemical properties of nano-materials as compared to that of the bulk materials. The magnetic semiconductor ferrites occupied a wide area of technological applications in microwave sets, radio and TV sets [1]. The transport properties of ferrites are very sensitive to the chemical composition, sintering temperature, sintering time, type and amount of substitution. The long-established applications of the ferrites include thin films, transformer applications, solar hydrogen production, multi-layer chip inductors, high-density magnetic recording, telecommunications, microwave devices, magnetic resonance imaging (MRI), sensors, catalysts etc. [2–5].

The metal spinel ferrites belong to the face centered (FCC) close packing structure of AB_2O_4 type having a unit cell with 32 Oxygen atoms in which A occupies tetrahedral site, B occupies octahedral cation site and O occupies the oxygen anion site in the normal spinel ferrite structure [6-7]. Ferrite nanoparticles show unusual magnetic properties which are not observed in bulk material such as single

[1] Department of Physics, G.M University Davanagere, Karnataka, India.
[2] Department of Engineering Physics, K. L. E Institute of Technology, Hubballi, 580027, Karnataka, India.
[3] Department of Studies & Research in Biochemistry, Tumkur University, Tumkur, 572137, Karnataka, India.
[4] PM Shri Kendriya Vidyalaya DIAT, Girinagar, Pune, 411025, India.
[5] Department of Physics, Anandibai Raorane Arts, Commerce and Science College, Vaibhavwadi, 416810, Maharashtra, India.

*Author to whom correspondence should be addressed:
nagarajubiochem@gmail.com (Shridhar N. Mathad);
drdeepakshirgaonkar@gmail.com (Deepak B. Shirgaonkar)

domain behavior and superparamagnetism [8]. The magnetism in ferrites originates from the magnetic moments at the metal ions. The interaction of these magnetic moments through the intervening O-2 ions is responsible for the observed magnetic behavior of ferrites. Among the spinel ferrite zinc ferrite has become a subject of interest because of its unique properties such as chemical and thermal stability, high electrical resistivity, low cost, low dielectric loss, high mechanical hardness and superior environmental stability and also the dependence of magnetic particle size on particle size [9–11]. The physical properties can be altered by introducing the different metallic ions results the cations distribution modification on the A-and B-sites [12–14].

The study of ferrites usually in most of the cases has been restricted to their structural, electrical and magnetic properties only, but the study of mechanical properties of ferrites has scientific importance due to their wide applications in industry and in research field because The Elastic constants are closely related to many important physical properties of solids [12–17]. Applications for nanotechnology are increasing quickly across a variety of fields including food sciences, biology and medicine (drug delivery and imaging). The delivery of medications and imaging agents using nanotechnology in medicine helps to accelerate uptake to target areas, change pharmacokinetic profiles, and improve the solubility of the drugs. Its simple preparation, low cost and high reactivity to chemical species make it a highly suitable material for use in gas sensors. The coagulation system's significance in vascular physiology and disease, as well as nanomaterial interactions with other system components, is a topic that is frequently discussed. Different methods, including the evaluation of re-calcification time (RT), prothrombin time (PT), and platelet aggregations, were used to assess the optimization of the anticoagulant activity of these ferrites in nanoparticulate systems, which limits the freedom of these macromolecules [18–22].

In the present study, the structural properties of the $Mg_{1-x}Co_xFe_2O_4$, $Mg_{1-x}Zn_xFe_2O_4$ and $Mg_{1-x}Ni_xFe_2O_4$ (x=0.15, 0.25 and 0.35) ferrites are explored by the XRD and SEM analysis. Also we discussed about anticoagulant properties of these ferrite samples by measuring re-calcification time, prothrombin time and platelet aggregation.

2. EXPERIMENTAL DETAILS

2.1 Materials

Aloe-vera, Methanol, 1, 4-diaminoanthraquinone, ortho-dichloromethane (ODCB), Triethyl amine (TEA) and Dimethyl formaldehyde (DMF), 4-Nitrophenol, and H_2O_2 were purchased from sigma Aldrich.

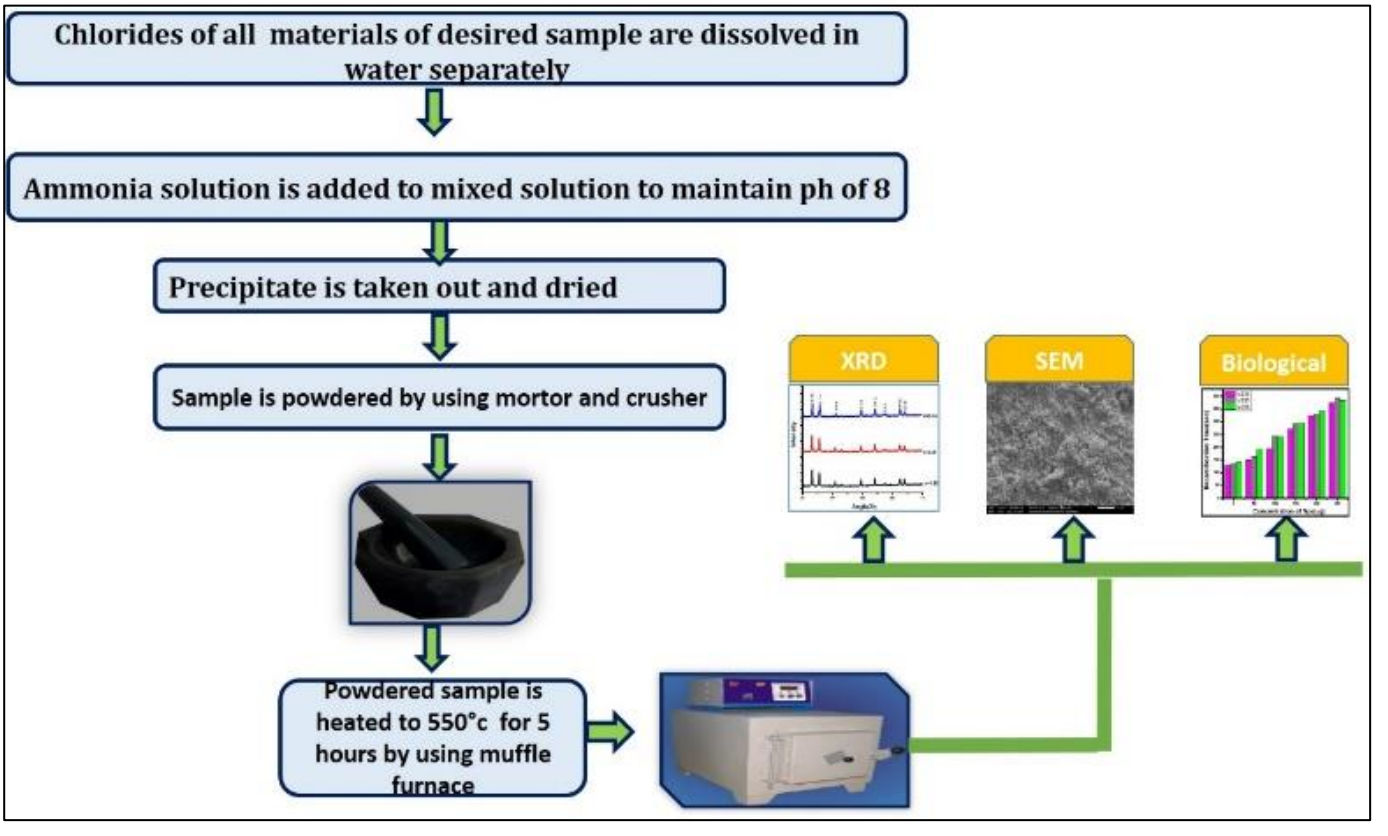

Fig. 1. Schematic of sample synthesis and further characterization.

2.1. Synthesis of ferrite composites

$Mg_{1-x}Co_xFe_2O_4$, $Mg_{1-x}Zn_xFe_2O_4$ and $Mg_{1-x}Ni_xFe_2O_4$ ferrite samples were fabricated using the economical, eco-friendly co-precipitation process. For preparing $Mg_{1-x}Zn_xFe_2O_4$ ferrite sample, analytical grade compounds of $MgCl_2 \cdot 4H_2O$, $ZnCl_2 \cdot 2H_2O$, and $FeCl_3 \cdot 6H_2O$ were individually dissolved in distilled water to create an ionic solution. Drop by drop, ammonia solution is added until the pH is 8. Metal hydroxides were created throughout this process, further formation of $Mg_{1-x}Zn_xFe_2O_4$ ferrites [23–26]. Powder was used from precipitate using a mortar and crusher. The well powdered sample is heated to 550°C for 6 hours by using muffle furnace. The similar procedure was followed for preparing $Mg_{1-x}Co_xFe_2O_4$ and $Mg_{1-x}Ni_xFe_2O_4$ ferrites. The schematic illustration of the synthesis route is as shown in Figure 1.

2.2. Characterizations

The surface morphology of the ferrite composites were analysed using a scanning electron microscope (SEM, JEOL Model JSM - 6390LV). The structural studies were done by X-ray diffractometer (Bruker AXS D8 Advance). The Amelung KC4A coagulometer was used to monitor re-calcification time.

3. RESULTS AND DISCUSSION

3.1. Structural properties

The X-ray diffraction patterns of $Mg_{1-x}Co_xFe_2O_4$, $Mg_{1-x}Zn_xFe_2O_4$ and $Mg_{1-x}Ni_xFe_2O_4$ (x=0.15, 0.25 and 0.35) ferrite samples are shown in Figure 2. The XRD pattern shows that all samples consist of single crystalline phase with cubic spinel structure. The diffraction angle range was 30–70° (2θ) with a step of 0.01° at a scan speed of 2°/min. The d-values and intensities of the diffraction maxima match the literature data of $MgFe_2O_4$ (JCPDC card #00-084-0542) [15, 27]. The diffraction peaks that correspond to the characteristic crystallographic planes of the spinel structure of ferrites are (220), (311), (400), (331), (422), (511), (440) and (531) [28, 29].

Crystal size (D) was computed using the Debye-Scherer equation as below:

$$D = \frac{0.9\ \lambda}{\beta\ cos\theta} \quad (1)$$

where β is the full width at half maximum of the peak.

Micro strain (ε) and dislocation density (ρ_D) can be computed utilizing the below equations:

$$\rho_D = \frac{1}{D^2} \quad (2)$$

$$\varepsilon = \frac{\beta \cos\theta}{4} \quad (3)$$

The lattice constant was observed in the range 8.323 to 8.353 Å, 8.328 to 8.351 Å and 8.315 to 8.366 Å for the $Mg_{1-x}Zn_xFe_2O_4$, $Mg_{1-x}Co_xFe_2O_4$ and $Mg_{1-x}Ni_xFe_2O_4$ ferrites respectively [12-13].

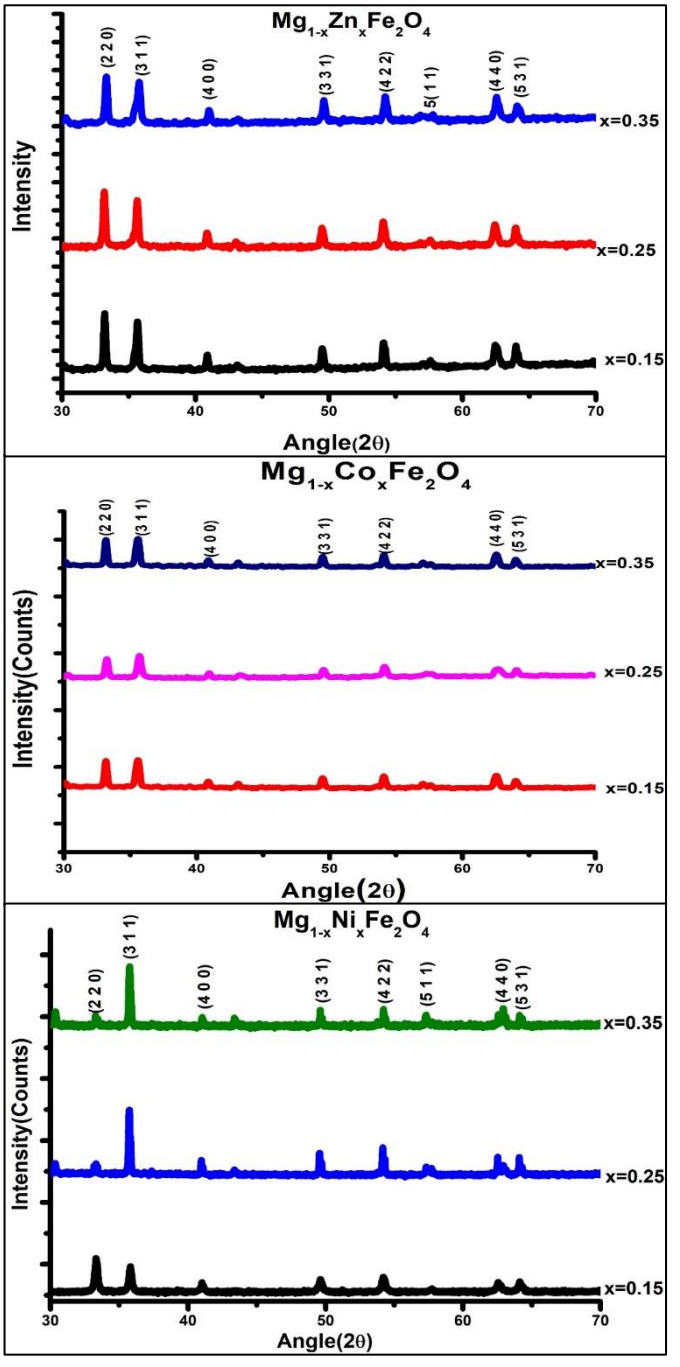

Fig. 2. XRD Patterns of $Mg_{1-x}Zn_xFe_2O_4$, $Mg_{1-x}Co_xFe_2O_4$ and $Mg_{1-x}Ni_xFe_2O_4$ (x=0.15, 0.25 and 0.35) ferrites.

Table 1 presents the detailed information for various concentrations, including the lattice parameter (a), unit cell volume (V), crystallite size (D), dislocation density (ρD), and microstrain (ε) of synthesized ferrite samples. Owing to Vegard's law, in $Mg_{1-x}Zn_xFe_2O_4$ ferrites, these parameters

were found to increase due to enhancement of zinc content; because Zn^{+2} ionic radius (0.74 Å) is greater than that of Mg^{+2} (0.72 Å) [13,19]. In case of $Mg_{1-x}Co_xFe_2O_4$ ferrites, these parameters were reduced due to enhancement of cobalt content; because Co^{+2} ionic radius (0.65 Å) is shorter than that of Mg^{+2} (0.72 Å) [30-31]. And in case of $Mg_{1-x}Ni_xFe_2O_4$ ferrites, these parameters were reduced due to enhancement of nickel content; because Ni^{+2} ionic radius (0.70 Å) is shorter than that of Mg^{+2} (0.72 Å) [32-33].

Table 1. Calculated values of lattice parameter (a), Volume of unit cell (V), crystallite size (D), Dislocation Density (ρ_D), micro strain (ε), and Grain sizes of $Mg_{1-x}Zn_xFe_2O_4$, $Mg_{1-x}Co_xFe_2O_4$and $Mg_{1-x}Ni_xFe_2O_4$ (x=0.15, 0.25 and 0.35) ferrites.

	$Mg_{1-x}Zn_xFe_2O_4$			$Mg_{1-x}Co_xFe_2O_4$			$Mg_{1-x}Ni_xFe_2O_4$		
Concentration X	0.15	0.25	0.35	0.15	0.25	0.35	0.15	0.25	0.35
Lattice parameter a (Å)	8.323	8.350	8.353	8.351	8.340	8.328	8.366	8.326	8.315
Volume of unit cell V (10^{-30} m)	576	582	582	582	580	577	585	577	574
Crystallite size D (nm)	27	27	30	34	32	25	24	41	39
Dislocation Density ρ_D ($X10^{14}$ m^{-2})	13.9	13.7	11.2	8.68	9.92	15.5	17.8	5.84	5.95
Micro Strain ε ($X10^{-3}$)	1.38	2.2	1.34	1.233	1.12	1.8	1.6	0.94	0.88
Grain size(μm)	3.745	3.984	4.229	4.67	5.08	4.034	4.887	3.252	3.946

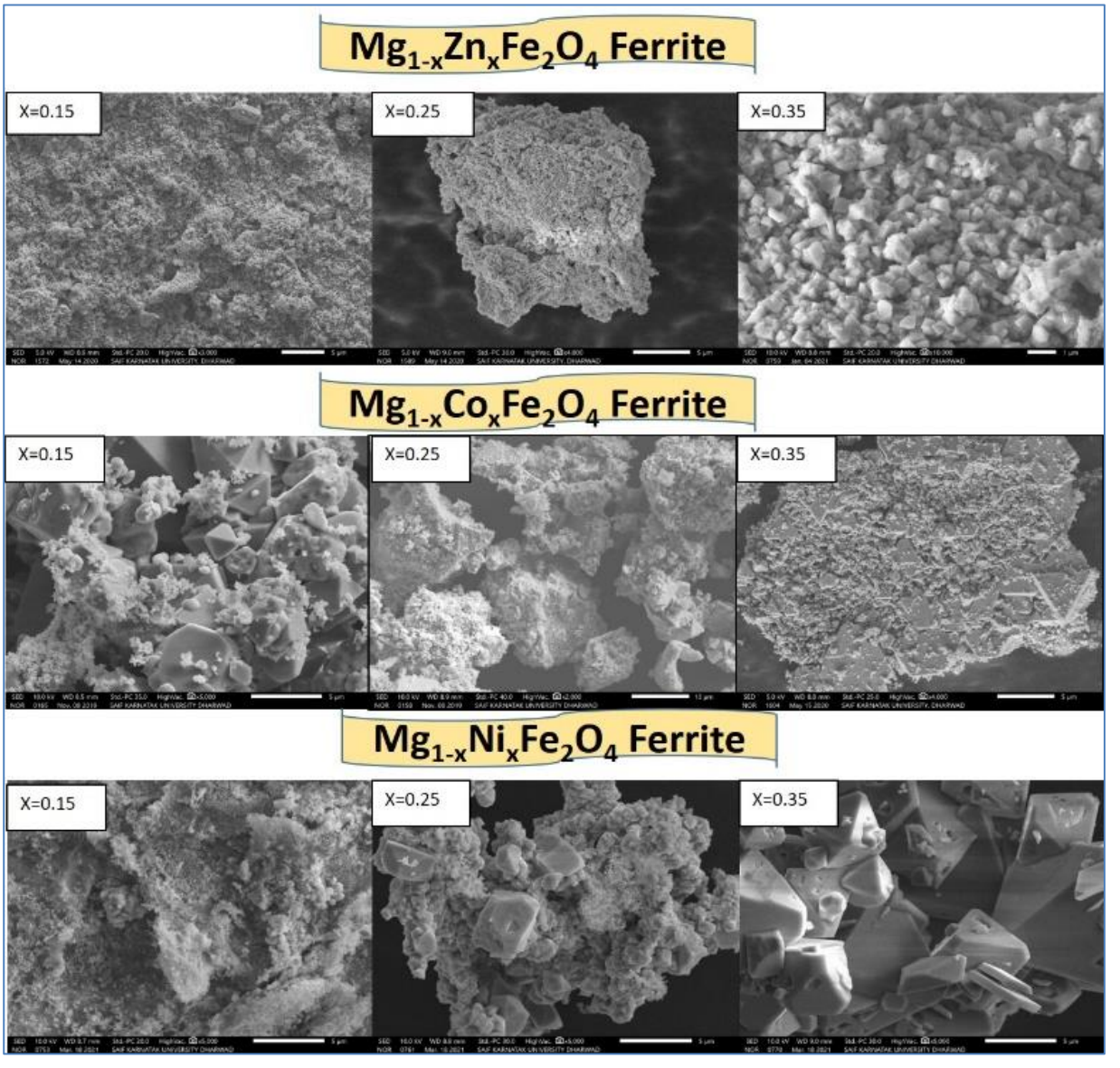

Fig. 3. SEM images of $Mg_{1-x}Zn_xFe_2O_4$, $Mg_{1-x}Co_xFe_2O_4$ and $Mg_{1-x}Ni_xFe_2O_4$ (x=0.15, 0.25 and 0.35) ferrites.

The morphological and microstructural analysis of $Mg_{1-x}Zn_xFe_2O_4$, $Mg_{1-x}Co_xFe_2O_4$ and $Mg_{1-x}Ni_xFe_2O_4$ (x=0.15, 0.25 and 0.35) ferrites were carried out by using JEOL Model JSM-6390LV. Figure 3 reveal that morphology changes continuously by varying the concentration of dopant and also shows that particles are agglomerated into large clusters [34-35]. The number of ferrites nanoparticles are nearly spherical in shape and the remaining are irregular polygon. The grain size of $Mg_{1-x}Zn_xFe_2O_4$, $Mg_{1-x}Co_xFe_2O_4$ and $Mg_{1-x}Ni_xFe_2O_4$ ferrites varied from 3.745 to 4.227 µm, 4.034 to 5.08 µm and 3.946 to 4.887 µm respectively as measured by Image J software and is presented in Table 1. The average grain size is larger than crystallite size measured by XRD, indicating greater amount of agglomeration during the process of nucleation. For $Mg_{1-x}Zn_xFe_2O_4$ ferrites, the grain size of the ferrite keeps growing with zinc doping since Zn^{+2} has a greater ionic radius (0.70 Å) than Mg^{+2} (0.72Å). For $Mg_{1-x}Co_xFe_2O_4$ ferrites, the grain size reduced with cobalt doping since Co^{+2} has a smaller ionic radius (0.65 Å) than that of Mg^{+2} (0.72Å), while in case of $Mg_{1-x}Ni_xFe_2O_4$ ferrites, the grain size reduced with nickel doping since Ni^{+2} has a smaller ionic radius (0.70 Å) than that of Mg^{+2} (0.72Å) [36-37].

3.2. Anticoagulant properties

Compared to other conventional systems, nanomaterials have a number of advantages. They can permeate cells and tissues to reach target organs, they can deliver drugs in a controlled manner. In particular, the performance of these nanomaterials can be assessed through anticoagulant assays. The ferrites can be used to prevent blood coagulation, they can be given to the people to reduce the chances of conditions such as strokes and heart attack. Ferrites offer more environment friendly pathway by shortening reaction time, and avoid harmful by-products. This will make them the best anticoagulants to be used in the medical field.

By monitoring re-calcification time in an Amelung KC4A coagulometer, the ability of ferrite nanoparticles' to enhance inhibition of rat plasma coagulation was evaluated (Mount Holly, NJ). The interval between adding the mixture and fibrin production is known as the re-calcification time. The ferrite samples were dissolved in a 0.154 mol/L NaCl solution for 24 hours before being collected [38-39]. Three test tubes each in eight separate groups of clean test tubes were used. The remaining seven groups each had ferrite samples, whereas the first group was left blank (10 mg each). Following a 2-minute incubation period at ambient temperature in a water bath for all samples, each test tube was filled with a pre-heated mixture of blood plasma (1.0 mL) and $CaCl_2$ solution (0.3 mL, 0.025 mol/L). The solution was gradually stirred with a stainless steel crotchet until fibrin was produced [40-41].

Re-calcification time is the clotting time of re-calcified plasma, its working principle is if an optimum amount of calcium is added to oxalated plasma containing platelets, coagulation results, and the time required for clotting has been termed as re-calcification time.

Prothrombin time (PT) is based on the principle that "in citrated plasma, addition of thromboplastin $CaCl_2$ allows for the formation of stable clot, the time required for the formation of stable clot is prothrombin time". Activated partial thromboplastin time (aPPT) is based on the principle that "in citrated plasma, the addition of platelet substitute and $CaCl_2$ allows for the formation of stable clot, the time required for the formation of stable clot is activated partial thromboplastin time. Platelet aggregation method checks how well platelets clump together to form blood clots. Upon the application of blood sample into polysteryne well, plasma proteins immediately adhere to the well surface resulting in platelet aggregation. Prothrombin time (PT) and activated partial thromboplastin time (aPTT) measurements show how ferrite materials affect the coagulant. 10 mg of the material was placed in test tubes with 0.5 mL of blood plasma. Thereafter, 0.25 mL of the $CaCl_2$ solution was added to these tubes, and the tubes were incubated at 37 °C until the temperature remained constant. The time of fibrin formation was recorded as aPTT. The time of blood plasma coagulation was noted as PT, When the PT agent was introduced in place of the $CaCl_2$. The platelet aggregation is the phenomenon through which blood platelets adhere to each other at the sites of injury. When nanoparticles come in contact with platelets, they will enhance platelet aggregation process.

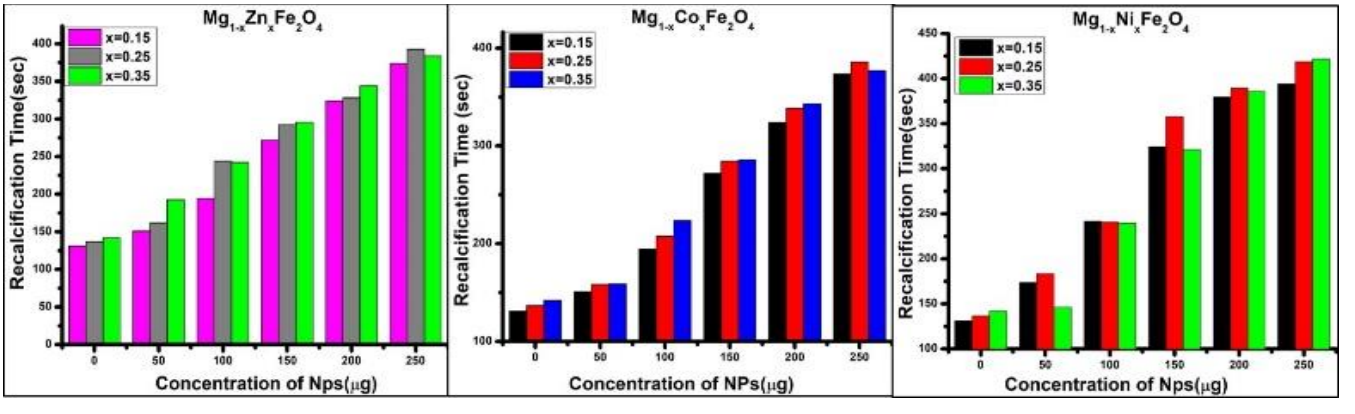

Fig. 4. Variation of Re-calcification time (sec) with concentration of NPs (µg) for $Mg_{1-x}Zn_xFe_2O_4$, $Mg_{1-x}Co_xFe_2O_4$ and $Mg_{1-x}Ni_xFe_2O_4$ (x=0.15, 0.25 and 0.35) ferrites.

Re-calcification time in a coagulometer was used to gauge the efficacy of $Mg_{1-x}Zn_xFe_2O_4$, $Mg_{1-x}Co_xFe_2O_4$ and $Mg_{1-x}Ni_xFe_2O_4$ (x=0.15, 0.25 and 0.35) ferrite nanoparticles to augment suppression of blood coagulation. The duration of the coagulation was measured in seconds. From the Table 2, we can observe that, compared to x=0.15 and x=0.25 ferrites, the re-calcification duration of x=0.35 ferrite samples is much longer, showing greater anticoagulant capability for all samples as depicted in Figure 4. This leads us to the conclusion that magnesium ferrite has better anticoagulant properties when Dopant content increased [39].

Further tests using the prothrombin time (PT) and activated partial thromboplastin time (aPTT) assays were run to confirm the NP's anticoagulant effects of $Mg_{1-x}Zn_xFe_2O_4$, $Mg_{1-x}Co_xFe_2O_4$ and $Mg_{1-x}Ni_xFe_2O_4$ (x=0.15, 0.25 and 0.35) ferrites. Figure 5 and Figure 6 depicts the variation of PT and aPPT with concentration of NPs respectively. From the Table. 2, aPTT and PT values of the x=0.35 materials were within the standard parameters, indicating that dopants had impact on the blood property, and they were longer than those of the x=0.15 and x=0.25 for all samples, indicating that x=0.35 ferrite had superior anticoagulant characteristics [39, 42].

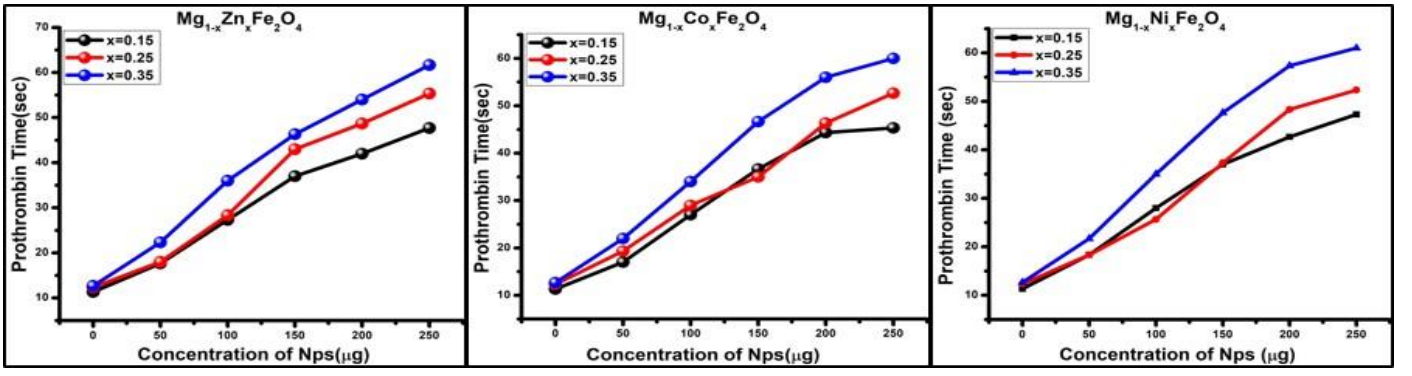

Fig. 5. Variation of Prothrombin time (sec) with concentration of Nps (µg) for $Mg_{1-x}Zn_xFe_2O_4$, $Mg_{1-x}Co_xFe_2O_4$ and $Mg_{1-x}Ni_xFe_2O_4$ (x=0.15, 0.25 and 0.35) ferrites.

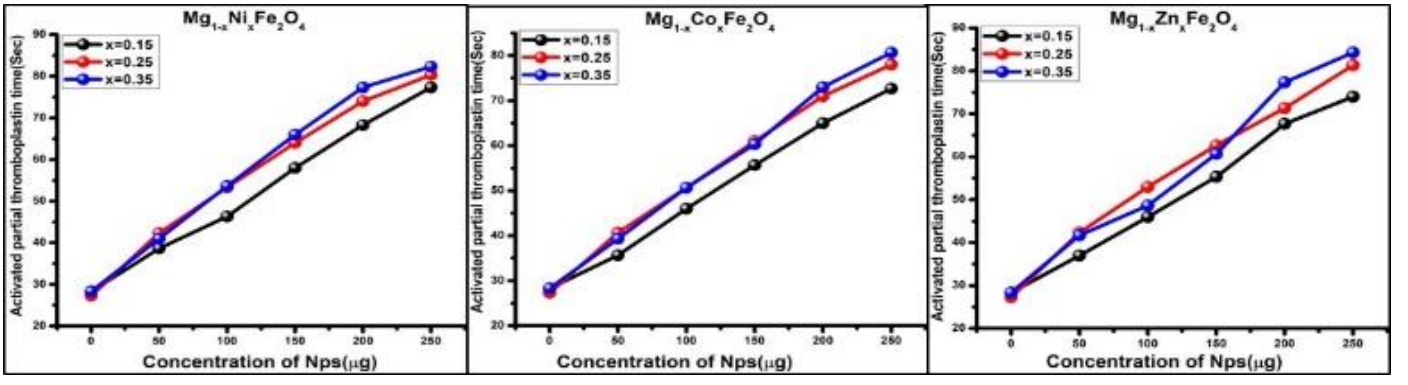

Fig. 6. Variation of Activated partial thromboplastin time (sec) with concentration of Nps (µg) for $Mg_{1-x}Zn_xFe_2O_4$, $Mg_{1-x}Co_xFe_2O_4$ and $Mg_{1-x}Ni_xFe_2O_4$ (x=0.15, 0.25 and 0.35) ferrites.

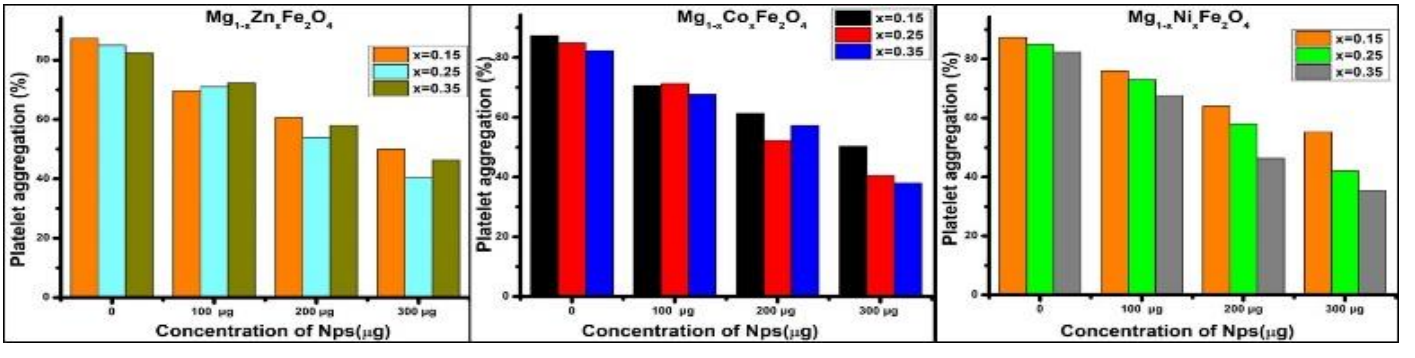

Fig. 7. Variation of Platelet aggregation (%) with concentration of Nps (µg) for $Mg_{1-x}Zn_xFe_2O_4$, $Mg_{1-x}Co_xFe_2O_4$ and $Mg_{1-x}Ni_xFe_2O_4$ (x=0.15, 0.25 and 0.35) ferrites.

Table 2. Measured values of Recalcification time, Activated partial thromboplastin time, Prothrombin time and Platelet aggregation percentage for $Mg_{1-x}Zn_xFe_2O_4$, $Mg_{1-x}Co_xFe_2O_4$ and $Mg_{1-x}Ni_xFe_2O_4$ (x=0.15, 0.25 and 0.35) ferrites.

	$Mg_{1-x}Zn_xFe_2O_4$,			$Mg_{1-x}Co_xFe_2O_4$			$Mg_{1-x}Ni_xFe_2O_4$		
Measurements (for NPs concentration= 250 µg)	**0.15**	**0.25**	**0.35**	**0.15**	**0.25**	**0.35**	**0.15**	**0.25**	**0.35**
Recalcification time (sec)	373	380	383	372	374	377	394	418	421
Activated partial thromboplastin time (aPTT) (sec)	74	81	84	72	78	80	77	80	82
Prothrombin time (sec)	47	55	62	45	52	60	46	51	61
Platelet aggregation percentage (%)	50	42	39	50	41	38	55	42	35

The figure 7 illustrates the $Mg_{1-x}Zn_xFe_2O_4$ ferrite's platelet aggregation %. From Table. 2, it has been observed that x=0.15 ferrites have a higher platelet aggregation percentage as compared to x=0.25 and x=0.35 ferrites in all samples. This is because nanoparticle size has an inverse relationship to the platelet aggregation percentage. Moreover, x=0.35 ferrites have improved anticoagulant behaviour because they cause less platelet aggregation [42,43].

4. CONCLUSION

A series of $Mg_{1-x}Zn_xFe_2O_4$, $Mg_{1-x}Co_xFe_2O_4$ and $Mg_{1-x}Ni_xFe_2O_4$ (x=0.15, 0.25 and 0.35) ferrites were prepared using the economical and environmentally friendly co-precipitation process. Sample's XRD analyses supported the discovery of single phase cubic spinel structure. The lattice constant was observed in the range 8.323 to 8.353 Å, 8.328 to 8.351 Å and 8.315 to 8.366 Å for the $Mg_{1-x}Zn_xFe_2O_4$, $Mg_{1-x}Co_xFe_2O_4$ and $Mg_{1-x}Ni_xFe_2O_4$ ferrites respectively. According to SEM pictures, ferrites are agglomerated and have surfaces with polygonal faces, such as cube, nearly spherical shaped grains. The grain size of $Mg_{1-x}Zn_xFe_2O_4$, $Mg_{1-x}Co_xFe_2O_4$ and $Mg_{1-x}Ni_xFe_2O_4$ ferrites varied from 3.745 to 4.227 µm, 4.034 to 5.08 µm and 3.946 to 4.887 µm respectively. Re-calcification time (RT), activated partial thromboplastin time (aPTT), and prothrombin time (PT) assays were employed to compute the capacity of all ferrite nanoparticles to augment inhibition of blood coagulation. The higher RT, aPPT, and PT values for the x=0.35 ferrites and lower platelet aggregation of the x=0.35 ferrites reveal that the anticoagulant properties of the x=0.35 ferrites are superior to those of the x=0.15 and x=0.25 ferrites for all samples. It is observed that the re-calcification time for MN ferrites is higher compared to other ferrites, also it shown a lesser platelet aggregation percentage for doping of x=0.35, they are good anticoagulant agents compared to MC and MZ ferrites.

CONFLICT OF INTEREST

The authors declare that there is no conflict of interests.

REFERENCES

[1] Wu, X.H., Li, L.Z., Zhong, X.X., Wang, R., Tu, X.Q., He, L. and Wang, F.H., **2019**. Effects of HfO_2 dopant on the structure, magnetic and electrical properties of NiZnCo ferrites. *Ceramics International*, 45(8), pp.10776-10781.

[2] Shahraki, R.R., Ebrahimi, M., Ebrahimi, S.S. and Masoudpanah, S.M., **2012**. Structural characterization and magnetic properties of superparamagnetic zinc ferrite nanoparticles synthesized by the coprecipitation method. Journal of Magnetism and Magnetic Materials, 324(22), pp.3762-3765.

[3] Hassadee, A., Jutarosaga, T. and Onreabroy, W., **2012**. Effect of zinc substitution on structural and magnetic properties of cobalt ferrite. Procedia Engineering, 32, pp.597-602.

[4] Yeary, L.W., Moon, J.W., Rawn, C.J., Love, L.J., Rondinone, A.J., Thompson, J.R., Chakoumakos, B.C. and Phelps, T.J., **2011**. Magnetic properties of bio-synthesized zinc ferrite nanoparticles. Journal of Magnetism and Magnetic Materials, 323(23), pp.3043-3048.

[5] Hsiang, H.I., Hsi, C.S., Tsai, C.Y. and Mei, L.T., **2015**. Cobalt-substitution effects on dielectric properties of CuZn ferrites. Ceramics International, 41(3), pp.4140-4144.

[6] Leonel, L.V., Righi, A., Mussel, W.N., Silva, J.B. and Mohallem, N.D.S., **2011**. Structural characterization of barium titanate–cobalt ferrite composite powders. Ceramics International, 37(4), pp.1259-1264.

[7] Ichiyanagi, Y., Kubota, M., Moritake, S., Kanazawa, Y., Yamada, T. and Uehashi, T., **2007**. Magnetic properties of Mg-ferrite nanoparticles. Journal of Magnetism and Magnetic Materials, 310(2), pp.2378-2380.

[8] Marinca, T.F., Chicinaș, I., Isnard, O., Pop, V. and Popa, F., **2011.** Synthesis, structural and magnetic characterization of nanocrystalline nickel ferrite—$NiFe_2O_4$ obtained by reactive milling. *Journal of Alloys and Compounds*, *509*(30), pp.7931-7936.

[9] Rendale, M.K., Mathad, S.N. and Puri, V., **2017**. Structural, mechanical and elastic properties of $Ni_{0.7-x}Co_xZn_{0.3}Fe_2O_4$ nano-ferrite thick films. *Microelectronics International*, 34(2), pp.57-63.

[10] Umapathy, G., Senguttuvan, G., John Berchmans, L. and Sivakumar, V., **2016**. Structural, dielectric and AC conductivity studies of Zn substituted nickel ferrites

prepared by combustion technique. *Journal of Materials Science: Materials in Electronics*, 27, pp.7062-7072.

[11] Srinivasan, G., Hayes, R., Devreugd, C.P., Laletsin, V.M. and Paddubnaya, N., **2005**. Dynamic magnetoelectric effects in bulk and layered composites of cobalt zinc ferrite and lead zirconate titanate. *Applied Physics A*, 80, pp.891-897.

[12] Zakaly, H.M., Issa, S.A., Saudi, H.A., Alharshan, G.A., Uosif, M.A.M. and Henaish, A.M.A., **2022**. Structure, Mössbauer, electrical, and γ-ray attenuation-properties of magnesium zinc ferrite synthesized co-precipitation method. *Scientific Reports*, *12*(1), p.15495.

[13] Kumar, D.R., Ahmad, S.I., Lincoln, C.A. and Ravinder, D., **2019.** Structural, optical, room-temperature and low-temperature magnetic properties of Mg–Zn nanoferrite ceramics. *Journal of Asian Ceramic Societies*, 7(1), pp.53-68.

[14] Kuru, M., Kuru, T.Ş., Karaca, E. and Bağcı, S., **2020**. Dielectric, magnetic and humidity properties of Mg–Zn–Cr ferrites. *Journal of Alloys and Compounds*, 836, p.155318.

[15] Vishwarup, R., Mathad, S.N., Altinawi, A., Altomali, R.H., Khan, A., Ibraheem, A.M., Alzahrani, K.A., Anand, B.C. and Gupta, V., **2024**. Effect of zinc substitution on structural, electrical, dielectric and magnetic properties of magnesium nano-ferrites prepared by co-precipitation route. *Inorganic Chemistry Communications*, p.112733.

[16] Tiwari, P., Verma, R., Kane, S.N., Tatarchuk, T. and Mazaleyrat, F., **2019.** Effect of Zn addition on structural, magnetic properties and anti-structural modeling of magnesium-nickel nano ferrites. *Materials Chemistry and Physics*, 229, pp.78-86.

[17] El Hiti, M.A., **1999**. Dielectric behaviour in Mg–Zn ferrites. *Journal of Magnetism and Magnetic Materials*, 192(2), pp.305-313.

[18] Choodamani, C., Nagabhushana, G.P., Rudraswamy, B. and Chandrappa, G.T., **2014**. Thermal effect on magnetic properties of Mg-Zn ferrite nanoparticles. *Materials Letters*, 116, pp.227-230.

[19] Gangaswamy, D.R.S., Bharadwaj, S., Varma, M.C., Choudary, G.S.V.R.K. and Rao, K.H., **2018**. Unusual increase in permeability in cobalt substituted Ni-Zn-Mg ferrites. *Journal of Magnetism and Magnetic Materials*, 468, pp.73-78.

[20] Da Silva, S.W., Nakagomi, F., Silva, M.S., Franco, A., Garg, V.K., Oliveira, A.C. and Morais, P.C., **2012**. Raman study of cations' distribution in $Zn_xMg_{1-x}Fe_2O_4$ nanoparticles. *Journal of Nanoparticle Research*, 14, pp.1-10.

[21] Yang, P., Liu, Z., Qi, H., Peng, Z. and Fu, X., **2019**. High-performance inductive couplers based on novel Ce^{3+} and Co^{2+} ions co-doped Ni-Zn ferrites. *Ceramics International*, 45(11), pp.13685-13691.

[22] Amaliya, A.P., Anand, S. and Pauline, S., **2018**. Investigation on structural, electrical and magnetic properties of titanium substituted cobalt ferrite nanocrystallites. *Journal of Magnetism and Magnetic Materials*, 467, pp.14-28.

[23] Jadhav, R.N., Mathad, S.N. and Puri, V., **2012**. Studies on the properties of $Ni_{0.6}Cu_{0.4}Mn_2O_4$ NTC ceramic due to Fe doping. *Ceramics International*, 38(6), pp.5181-5188.

[24] Manikandan, V., Sikarwar, S., Yadav, B.C. and Mane, R.S., **2018**. Fabrication of tin substituted nickel ferrite (Sn-$NiFe_2O_4$) thin film and its application as opto-electronic humidity sensor. *Sensors and Actuators A: Physical*, 272, pp.267-273.

[25] Vishwaroop, R. and Mathad, S.N., **2020**. Synthesis, structural, WH plot and size-strain analysis of nano cobalt doped $MgFe_2O_4$ ferrite. *Science of Sintering*, 52(3), pp.349-358.

[26] Joshi, S., Kumar, M., Pandey, H., Singh, M. and Pal, P., **2018**. Structural, magnetic and dielectric properties of Gd^{3+} substituted $NiFe_2O_4$ nanoparticles. *Journal of Alloys and Compounds*, 768, pp.287-297.

[27] Wang, Z., Lazor, P., Saxena, S.K. and O'Neill, H.S.C., **2002**. High pressure Raman spectroscopy of ferrite $MgFe_2O_4$. *Materials Research Bulletin*, 37(9), pp.1589-1602.

[28] Mund, H.S. and Ahuja, B.L., **2017.** Structural and magnetic properties of Mg doped cobalt ferrite nano particles prepared by sol-gel method. *Materials Research Bulletin*, *85*, pp.228-233.

[29] Majee, M.K., Nigam, A.K. and Bhobe, P.A., **2019.** Comparison of local crystal structure and magnetic properties of cation substituted $LiNiO_2$ compositions. *Materials Research Bulletin*, *116*, pp.143-152.

[30] Mohanty, D., Naik, A.U., Nayak, P.K., Behera, B. and Satpathy, S.K., **2021.** Structural and electrical properties of magnesium-doped $CoFe_2O_4$. *Powder Metallurgy and Metal Ceramics*, 59, pp.507-514.

[31] Vishwarup, R. and Mathad, S.N., **2020**. Facile Synthesis of Nano Mg-Co Ferrites (x= 0.15, 0.20, 0.25, 0.30, 0.35, and 0.40) via Co-precipitation Route: Structural Characterization. *Materials International*, 2(4), pp.0471-0476.

[32] Vivekanandhan, S., Venkateswarlu, M. and Satyanarayana, N., **2004**. Effect of ethylene glycol on polyacrylic acid based combustion process for the synthesis of nano-crystalline nickel ferrite ($NiFe_2O_4$). *Materials Letters*, *58*(22-23), pp.2717-2720.

[33] Gandhad, S.S., Patil, P.M., Mathad, S.N., Hublikar, L.V., Jeergal, P.R. and Pujar, R.B., **2019.** Effect of aluminum doping on structural and mechanical properties of Ni–Mg ferrites. *International Journal of Self-Propagating High-Temperature Synthesis*, 28(4), pp.271-273.

[34] Khemalapure, S.S., Hosamani, P.L., Mathad, S.N., Pujar, A.S., Hiremath, C.S., Jeeragal, P.R., Pawar, S.S. and Pujar, R.B., **2019**. Synthesis, structural and dielectric properties of Ni–Zn–Cu ferrites. *Advanced Science, Engineering and Medicine*, 11(5), pp.375-382.

[35] Andjelković, L., Šuljagić, M., Lakić, M., Jeremić, D., Vulić, P. and Nikolić, A.S., **2018**. A study of the structural and morphological properties of Ni–ferrite, Zn–ferrite and Ni–Zn–ferrites functionalized with starch.

Ceramics International, 44(12), pp.14163-14168.

[36] Gole, D.A., Kapatkar, S.B., Mathad, S.N. and Chavan, R.R., **2021**. Facile co-precipitation route for magnesium ferrites nanostructure: Synthesis, influence of pH variation on structural properties. *Science of Sintering*, 53(1), pp.67-78.

[37] Thomas, N., Shimna, T., Jithin, P.V., Sudheesh, V.D., Choudhary, H.K., Sahoo, B., Nair, S.S., Lakshmi, N. and Sebastian, V., **2018.** Comparative study of the structural and magnetic properties of alpha and beta phases of lithium ferrite nanoparticles synthesized by solution combustion method. *Journal of Magnetism and Magnetic Materials*, 462, pp.136-143.

[38] Li, T., Li, D., Xu, X., Zhu, Y., Phiri, M., Ji, S., Shu, C. and Ding, L., **2020.** A simple injectable peptide-based hydrogel of tanshinone IIA for antioxidant and anticoagulation. *Journal of Drug Delivery Science and Technology*, 58, p.101532.

[39] da Silva, L.C., Garcia, T., Mori, M., Sandri, G., Bonferoni, M.C., Finotelli, P.V., Cinelli, L.P., Caramella, C. and Cabral, L.M., **2012**. Preparation and characterization of polysaccharide-based nanoparticles with anticoagulant activity. *International Journal of Nanomedicine*, pp.2975-2986.

[40] Kargl, R. and Kleinschek, K.S., **2020**. How can we understand the influence of nanoparticles on the coagulation of blood?. *Nanomedicine*, 15(20), pp.1923-1926.

[41] Ilinskaya, A.N. and Dobrovolskaia, M.A., **2013**. Nanoparticles and the blood coagulation system. Part I: benefits of nanotechnology. *Nanomedicine*, 8(5), pp.773-784.

[42] Xu, X.R., Zhang, D., Oswald, B.E., Carrim, N., Wang, X., Hou, Y., Zhang, Q., Lavalle, C., McKeown, T., Marshall, A.H. and Ni, H., **2016**. Platelets are versatile cells: New discoveries in hemostasis, thrombosis, immune responses, tumor metastasis and beyond. *Critical reviews in Clinical Laboratory Sciences*, *53*(6), pp.409-430.

[43] Zia, F., Kendall, M., Watson, S.P. and Mendes, P.M., **2018**. Platelet aggregation induced by polystyrene and platinum nanoparticles is dependent on surface area. *RSC Advances*, 8(66), pp.37789-37794.

